

Electronic read-out of a single nuclear spin using a molecular spin transistor

Romain Vincent¹, Svetlana Klyatskaya², Mario Ruben^{2,3}, Wolfgang Wernsdorfer¹ & Franck Balestro¹

Quantum control of individual spins in condensed-matter devices is an emerging field with a wide range of applications, from nanospintronics^{1,2} to quantum computing³. The electron, possessing spin and orbital degrees of freedom, is conventionally used as the carrier of quantum information in proposed devices^{4,5,6,7,8,9}. However, electrons couple strongly to the environment, and so have very short relaxation and coherence times. It is therefore extremely difficult to achieve quantum coherence and stable entanglement of electron spins. Alternative concepts propose nuclear spins as the building blocks for quantum computing¹⁰, because such spins are extremely well isolated from the environment and less prone to decoherence. However, weak coupling comes at a price: it remains challenging to address and manipulate individual nuclear spins^{11,12,13,14}. Here we show that the nuclear spin of an individual metal atom embedded in a single-molecule magnet can be read out electronically. The observed long lifetimes (tens of seconds) and relaxation characteristics of nuclear spin at the single-atom scale open the way to a completely new world of devices in which quantum logic may be implemented.

Single-shot read-out of a single nuclear spin has remained elusive until the past few years, when it was achieved on a single nitrogen-vacancy defect centre in diamond¹⁵. The use of single-molecule magnets (SMMs) has also been proposed as a structural basis for nanospintronics¹⁶ and quantum information⁹. The argument in favour of molecular building blocks for quantum computing is based on the possibility of synthesizing billions of perfectly identical SMMs, which can be integrated in devices by bottom-up approaches and for which the intrinsic magnetic properties and the environment can be chemically engineered. Moreover, experiments on an assembly of SMMs have already shown that: SMMs are characterized by a large

spin ground state combined with uniaxial magnetic anisotropy leading to two stable spin orientations; quantum phenomena such as quantum tunnelling of the magnetization (QTM)^{17,18} and quantum phase interference¹⁹ can be observed; and spin-state oscillations can be made coherent^{20,21} for a time on the order of 1 μ s. To achieve a longer coherence time, experiments must be done on the single-molecule level, avoiding interactions between SMMs. However, it is still difficult to detect single spin states in an SMM. Towards this goal, transport measurements have been made using scanning tunnelling microscopy (STM)^{22,23}, and SMMs have been studied in a transistor-like configuration using electromigrated junctions^{24,25} or carbon-nanotube transistors²⁶. So far, only signatures accounting for the electronic magnetic moment have been addressed, and there has been no quantitative comparison with the expected theoretical magnetic behaviour of an individual SMM.

Here, transport measurements taken through a single bis(phthalocyaninato)terbium(III) SMM (TbPc₂, Fig. 1) are studied in a three-terminal geometry obtained by electromigration²⁷. TbPc₂ is a lanthanide SMM, in which the magnetic moment is carried by a single Tb³⁺ metal ion sandwiched between two organic phthalocyanine (Pc) ligands. We used this particular SMM for the several reasons. It has been reported that TbPc₂ SMMs conserve both their structural integrity and their magnetic properties even when sublimated at 820 K on a copper surface²⁸. The redox state of the Tb³⁺ ion is very stable; that is, it is very unlikely that a current can flow through the Tb³⁺ ion (see Supplementary Information). The two Pc ligands have a conjugated π system, which can easily conduct electrons. Owing to strong spin-orbit coupling and the Pc ligand fields, TbPc₂ has a magnetic ground state of $J = 6$ and a strong uniaxial magnetic anisotropy (Ising-like, Fig. 1a). The ground-state doublet $J_z = \pm 6$ is well isolated

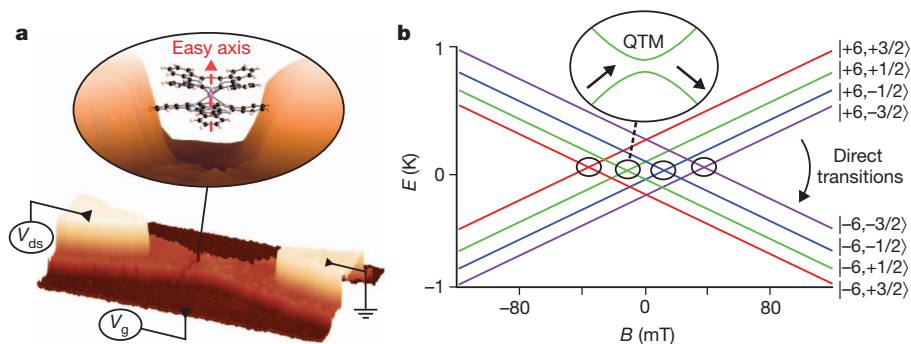


Figure 1 | Geometry of the molecular spin transistor and magnetization reversal processes. **a**, Three-dimensional extrapolation of a scanning-electron-microscope image showing the most favourable structure of the single-molecule-based transistor. A schematic zoom into the nano gap shows the molecular structure of the TbPc₂ SMM and its easy axis. The charge state of the ligand read-out dot can be controlled by the gate voltage, V_g , and the voltage difference between the electrodes is controlled through the drain-source voltage, V_{ds} . **b**, Zeeman diagram presenting the energy, E , of the two ground

states, $J_z = \pm 6$, as a function of the magnetic field (B). The two ground states are each split into four different sub-states owing to the hyperfine coupling with the nuclear spin of $I = 3/2$. Coloured lines denote the I_z components of the nuclear spin states: purple, $-3/2$; blue, $-1/2$; green, $1/2$; and red, $3/2$. Two processes are responsible for the magnetization reversal. In small magnetic fields, QTM can occur at the avoided energy-level crossings with the same I_z but opposite J_z , indicated by the black circles. In higher fields, a direct relaxation process can lead to the reversal of J .

¹Institut Néel, CNRS et Université Joseph Fourier, BP 166, F-38042 Grenoble Cedex 9, France. ²Institute of Nanotechnology, Karlsruhe Institute of Technology, 76344 Eggenstein-Leopoldshafen, Germany. ³Institut de Physique et Chimie des Matériaux de Strasbourg, CNRS-Université de Strasbourg, 67034 Strasbourg, France.

from the excited states by an energy gap of a few hundred kelvin²⁹. The excited states can thus be neglected for experiments carried out at low temperatures (less than 5 K) and small magnetic fields (less than 10 T). The ligand fields also induce transverse magnetic anisotropy, which is responsible for the coupling of the two states of the doublet $J_z = \pm 6$, so that energy-level crossings are avoided²⁹ (see the black circles in the Zeeman diagram of Fig. 1b). Finally, because of strong hyperfine coupling with the nuclear spin $I = 3/2$ of the Tb^{3+} ion, each ground state $J_z = \pm 6$ is split into four states (Fig. 1b).

Within the low-temperature regime, the magnetization reversal of a TbPc_2 SMM takes place through two different processes. In small magnetic fields, QTM at the four avoided level crossings (see above) is the main mechanism²⁹, whereas in higher magnetic fields, relaxation processes can be direct, involving non-coherent tunnelling events combined with phonon emission. QTM of a TbPc_2 SMM has been observed in a supramolecular carbon-nanotube SMM spin-valve geometry²⁶, but the signature of the hyperfine coupling could not be accessed, owing to the background noise induced by the surrounding TbPc_2 SMMs. Here, we show that by detecting the reversal of the electronic magnetic moment of the TbPc_2 SMM, we can produce an electronic read-out of the four nuclear spin states of a single Tb^{3+} ion with high efficiency and in perfect quantitative agreement with the theoretical predictions²⁹. Furthermore, we estimate the lifetimes and the temperature of a single nuclear spin.

Transport measurements through a single TbPc_2 SMM have been taken previously by scanning tunnelling spectroscopy (STS) experiments²², for which electronic transport occurred through the Pc ligands and exhibited Coulomb blockade and Kondo effects depending on its charge state (spin states $S = 0$ or $1/2$). However, no signature of the magnetic moment carried by the Tb^{3+} ion was observed in this experiment. To detect the reversal of the magnetic moment, and to produce the electronic read-out of the Tb^{3+} nuclear spin states, we

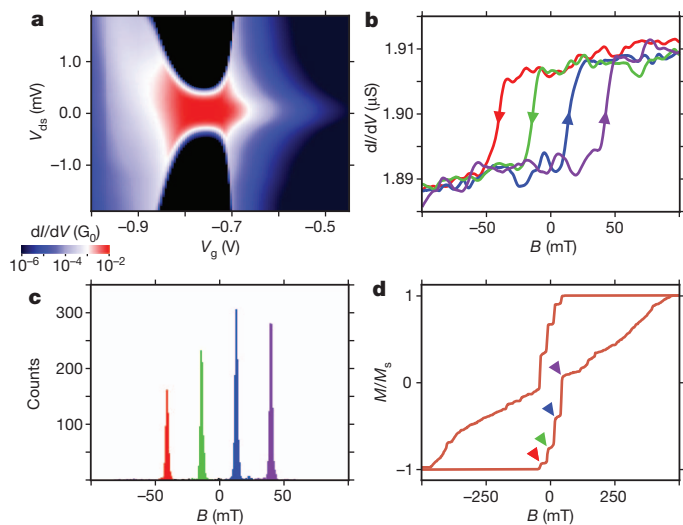


Figure 2 | Conductance characteristics and electronic read-out procedure. **a**, Stability diagram of the Pc read-out quantum dot exhibiting the differential conductance, dI/dV , in units of the quantum of conductance, G_0 , as a function of gate voltage, V_g , and bias voltage, V_{ds} , at 0.1 K. **b**, dI/dV measurements for a given working point ($V_g = -0.9$ V; $V_{ds} = 0$ V) as a function of the magnetic field, B . The arrows indicate the field-sweep direction. Abrupt jumps in the differential conductance, attributed to the switching of the Tb^{3+} magnetic moment, are visible for all traces of B , showing a clear hysteresis in the dI/dV characteristics. **c**, Histogram of switching field values obtained for 11,000 field sweeps showing four preferential field values that are assigned to QTM events. **d**, Normalized hysteresis loop of a single TbPc_2 SMM obtained by integration of 1,000 field sweeps and performed for trace and retrace on a larger magnetic-field range than in **c**. The four arrows on the trace curve show the four preferential field values associated to QTM (red, -40 mT; green, -14 mT; blue, 14 mT; purple, 40 mT).

inserted the TbPc_2 SMM directly into a gold junction obtained by the electromigration technique (see Fig. 1a and Methods). The differential conductance, dI/dV , as the function of the drain-source voltage, V_{ds} , and the gate voltage, V_g , is presented in Fig. 2a. It exhibits a single charge-degeneracy point with a weak spin $S = 1/2$ Kondo effect. A detailed study of the Kondo peak as a function of the applied magnetic field is presented in the Supplementary Information. A ferromagnetic exchange interaction of about 0.35 T was measured between the spin $1/2$ of the quantum dot and the magnetic moment carried by the Tb^{3+} ion. Alternative coupling mechanisms (dipolar, magneto-Coulomb, mechanical, flux) are discussed in the Supplementary Information, but the relatively high value of the exchange interaction means that it should be the major contribution to the coupling mechanism, and that the quantum dot is spatially located close to the Tb^{3+} ion. This is indirect proof that the electronic transport occurs through the aromatic Pc ligands, and that the most favourable geometric configuration is the one depicted in Fig. 1a. To summarize: the Pc ligands form a molecular quantum dot and the anisotropic magnetic moment of the Tb^{3+} ion is coupled to the electron path only indirectly, mainly through a ferromagnetic exchange interaction; the presence of a gate allows fine-tuning from the Coulomb blockade to the Kondo regime of the molecular quantum dot; the magnetic properties of the Tb^{3+} ion are then independent of the charge state of the Pc quantum dot (see Supplementary Information); and owing to the exchange coupling, we can use the Pc ligands as a read-out quantum dot to detect the reversal of the electronic magnetic moment carried by the Tb^{3+} ion spin dot.

To produce the electronic read-out of the single nuclear spin carried by the spin dot, we chose experimental conditions close to the charge-degeneracy point ($V_g = -0.9$ V and $V_{ds} = 0$ V in Fig. 2a, see Supplementary Information). When sweeping the magnetic field from negative to positive values, we observed a single abrupt jump of the differential conductance, which reversed when we swept the field in the opposite direction (Fig. 2b). Our detailed studies (see below) showed that these jumps can be accounted for by the reversals of the Tb^{3+} magnetic moment, which slightly influence the chemical potential of the read-out quantum dot through the magnetic interactions

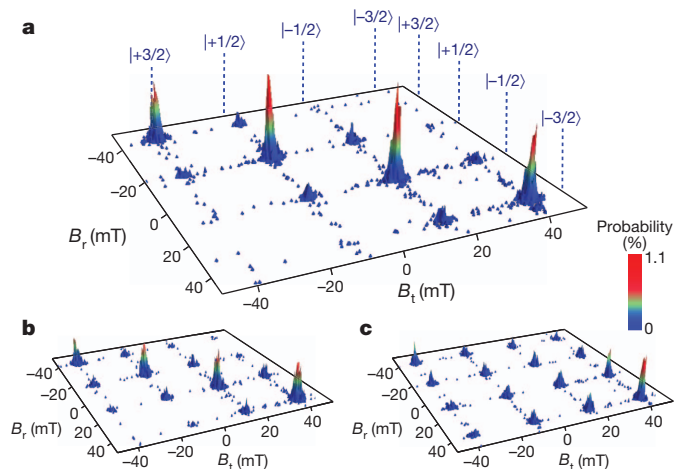


Figure 3 | Transition matrix of the QTM events as a function of the waiting time. The switching fields of the Tb^{3+} magnetic moment of subsequent field sweeps are plotted in two-dimensional histograms for three waiting times, t_w : **a**, $t_w = 0$ s; **b**, $t_w = 20$ s; and **c**, $t_w = 50$ s. The two axes correspond to the trace and retrace field sweeps, B_t and B_r , respectively. Two successive measurements with the same nuclear spin states are situated on the diagonal of the matrix, whereas the off-diagonal positions correspond to nuclear spin-state changes of $\Delta m_I = \pm 1, \pm 2$ and ± 3 . The predominance of diagonal terms up to $t_w = 20$ s indicates the long level lifetime of the nuclear spin states. For $t_w = 50$ s, the diagonal terms vanish owing to nuclear spin-flip processes. Furthermore, the high amplitude of the bottom-right ($B_t = B_r = 40$ mT) matrix element accounts for the relaxation of the nuclear spin towards a thermal equilibrium.

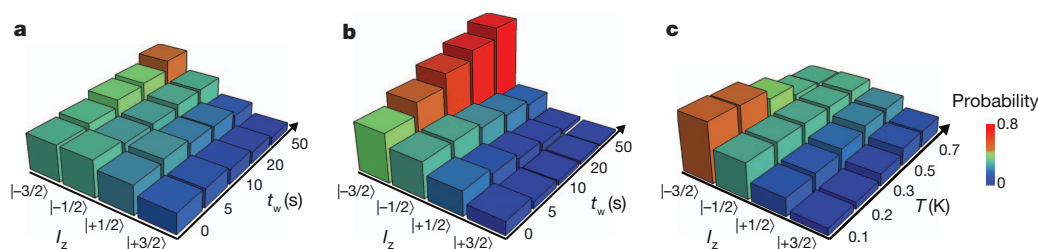


Figure 4 | Spin-flip dynamics and nuclear spin-state occupancy of the Tb^{3+} nuclear spin states. Evolution of the nuclear spin-state occupancy as a function of the waiting time, t_w , for two different working points: **a**, gate voltage $V_g = -0.9$ V; and **b**, $V_g = -0.1$ V (both at bias voltage $V_{ds} = 0$ V). The

(see Supplementary Information). We took subsequent measurements of the reversal as a function of the magnetic-field angle in a dilution refrigerator equipped with a home-made three-dimensional vector magnet. We were thus able to align the field-sweep direction accurately along the easy axis of the TbPc_2 SMM (see Supplementary Information).

We obtained the reversal statistics of the magnetization by sweeping the magnetic field back and forth at 0.05 T s^{-1} and measuring histograms of the switching fields. We present a typical example in Fig. 2c, showing four preferential magnetic-field values. These are in perfect quantitative agreement with theoretical predictions²⁹ of QTM of a Tb^{3+} magnetic moment at the four avoided energy-level crossings with the nuclear spin states $|3/2\rangle$, $|1/2\rangle$, $|-1/2\rangle$ and $|-3/2\rangle$ (Fig. 1b). Moreover, the histograms of the four switching fields do not overlap; this shows the high efficiency of this electronic read-out procedure. The field integration of the normalized switching histograms yields the magnetic hysteresis loop (Fig. 2d), which is in excellent accordance with micro-SQUID measurements of assemblies of TbPc_2 SMMs (see Supplementary Information and ref. 29). In higher magnetic fields, the reversal of the magnetization occurs stochastically, as predicted for a direct relaxation process involving a non-coherent tunnelling event combined with a phonon emission.

The lifetimes of the four nuclear spin states could be measured by studying the correlations between subsequent measurements as a function of the waiting time, t_w , between field sweeps. Figure 3 presents two-dimensional histograms (transition matrices) obtained from 22,000 field sweeps. The two axes correspond to the trace and retrace field sweeps, B_t and B_r . Two subsequent measurements with the same nuclear spin states are situated on the diagonal of the matrix; the off-diagonal positions correspond to nuclear spin state changes of $\Delta m_I = \pm 1$, ± 2 , and ± 3 . For zero waiting time ($t_w = 0$ s, Fig. 3a), the diagonal positions are predominant, highlighting the robustness of the nuclear spin states; that is, indicating long level lifetimes for the individual Tb^{3+} nuclear spin states. The diagonal positions persist even for a waiting time of $t_w = 20$ s (Fig. 3b). However, for $t_w = 50$ s, the off-diagonal positions start to be populated, which suggests the occurrence of nuclear spin-flip processes during the waiting time (Fig. 3c). From this series of measurements, we conclude that the level lifetime of the nuclear spin states is on the order of tens of seconds, confirming that the invasiveness of the measurement procedure is low (see Supplementary Information).

More detailed insight into the spin-flip dynamics of an individual nuclear spin can be gained by measuring the population of nuclear spin states as a function of waiting time and temperature (Fig. 4). To this end, we determined the nuclear spin-state occupancy for two different working points corresponding to two different charge states of the read-out quantum dot ($V_g = -0.9$ V in Fig. 4a and $V_g = -0.1$ V in Fig. 4b, both at $V_{ds} = 0$ V). It is clear that the state occupancy, relaxing towards a thermal equilibrium, depends heavily on the transport characteristics (the current flowing through the Pc quantum dot and/or the electrostatic environment modulated by the gate voltage). Indeed, the electron tunnelling through the Pc-ligands read-out dot gives rise to

measurements clearly show that the populations evolve towards different thermal equilibria. **c**, Spin dynamics for a fixed waiting time of 10 s, as a function of temperature, T . With increasing temperature, the population of the different spin states evolves towards equal occupancy.

small fluctuations of the local electric field, which could modify nuclear spin-flip processes through the quadrupole interaction³⁰. A detailed study addressing this problem is in progress, and beyond the scope of the work presented here. We also determined the population of nuclear spin states as a function of the temperature (Fig. 4c). The strong temperature dependence of this occupancy demonstrates that a single nuclear spin can be thermalized down to at least 0.2 K, which is close to the electronic temperature of our dilution refrigerator (0.08 K).

In conclusion, we have performed electronic transport studies on a TbPc_2 SMM in a transistor-like set-up, taking measurements of a single nuclear spin. Our experimental read-out procedure relies on the highly efficient detection of the QTM of the electronic magnetic moment at particular values of the magnetic field corresponding to the four avoided energy-level crossings; this is in perfect quantitative agreement with theoretical predictions. Using this procedure, the dynamics of the four different nuclear spin states of a single Tb^{3+} ion could be electronically determined. The observation of energy-level lifetimes on the order of tens of seconds opens the way to coherent manipulations of a single nuclear spin. Moreover, because of the different energy-level spacing that originates from the nuclear quadrupole interaction term (see Supplementary Information), this particular device is presumed to be an excellent candidate to perform the Grover algorithm. Indeed it has been proposed that the coherent manipulation of a nuclear spin $I = 3/2$ can be performed through a multiphoton process using this algorithm³¹. It was predicted that the greater the quadrupolar constant, the better the implementation of the algorithm would be. Note that the value presented in ref. 31 was three orders of magnitude smaller than the value presented here ($P = 0.013 \text{ cm}^{-1}$). Thus, the demonstrated possibility of addressing and detecting single nuclear spin states using the QTM of SMMs, in combination with the observation of long energy-level lifetimes, opens up a bright new world of nanospintronics with integrated memory, logics and possibly quantum logics.

METHODS SUMMARY

The single-molecule transistor was prepared by blow-drying a dilute toluene solution of the TbPc_2 molecule onto a gold nanowire on an Au/HfO₂ gate fabricated through atomic-layer deposition. Before the solution was blow-dried, the electrodes were cleaned with acetone, ethanol, isopropanol solution and oxygen plasma. The connected sample was enclosed in a high-frequency, low-temperature filter, consisting of a thermocoax microwave filter and π filters, anchored to the mixing chamber of a dilution refrigerator with a base temperature of about 0.05 K. The molecule-coated nanowire was then broken by electromigration, using a voltage ramp at 4 K. The electromigration technique used real-time electronics to increase the yield of coupling a single molecule to the electrodes.

Transport measurements were taken using a lock-in amplifier in a dilution refrigerator with an electronic temperature of about 0.08 K. It was equipped with a home-made three-dimensional vector magnet, allowing us to sweep the magnetic field in three dimensions at rates up to 0.2 T s^{-1} .

Received 9 April; accepted 19 June 2012.

1. Awschalom, D. D., Loss, D. & Samarth, N. *Semiconductor Spintronics and Quantum Computation* (Springer, 2002).

2. Zutic, I., Fabian, J. & Das Sarma, S. Spintronics: fundamentals and applications. *Rev. Mod. Phys.* **76**, 323–410 (2004).
3. Nielsen, M. A. & Chuang, I. L. *Quantum Computation and Quantum Information* (Cambridge Univ. Press, 2000).
4. Loss, D. & DiVincenzo, D. P. Quantum computation with quantum dots. *Phys. Rev. A* **57**, 120–126 (1998).
5. Imamoglu, A. *et al.* Quantum information processing using quantum dot spins and cavity QED. *Phys. Rev. Lett.* **83**, 4204–4207 (1999).
6. Eble, B. *et al.* Hole–nuclear spin interaction in quantum dots. *Phys. Rev. Lett.* **102**, 1–4 (2009).
7. Jelezko, F., Gaebel, T., Popa, I., Gruber, A. & Wrachtrup, J. Observation of coherent oscillations in a single electron spin. *Phys. Rev. Lett.* **92**, 1–4 (2004).
8. Vrijen, R. *et al.* Electron-spin-resonance transistors for quantum computing in silicon-germanium heterostructures. *Phys. Rev. A* **62**, 1–10 (2000).
9. Leuenberger, M. N. & Loss, D. Quantum computing in molecular magnets. *Nature* **410**, 789–793 (2001).
10. Kane, B. E. A silicon-based nuclear spin quantum computer. *Nature* **393**, 133–137 (1998).
11. Chuang, I. L., Gershenfeld, N. & Kubinec, M. Experimental implementation of fast quantum searching. *Nature* **393**, 143–146 (1998).
12. Chuang, I. L., Vandersypen, L. M. K., Zhou, X., Leung, D. W. & Lloyd, S. Experimental realization of a quantum algorithm. *Phys. Rev. Lett.* **80**, 3408–3411 (1998).
13. DiVincenzo, D. P. Two-bit gates are universal for quantum computation. *Phys. Rev. A* **51**, 1015–1022 (1995).
14. Berman, G. P., Doolen, G. D., Hammel, P. C. & Tsifrinovich, V. I. Solid-state nuclear-spin quantum computer based on magnetic resonance force microscopy. *Phys. Rev. B* **61**, 14694–14699 (2000).
15. Neumann, P. *et al.* Single-shot readout of a single nuclear spin. *Science* **329**, 542–544 (2010).
16. Bogani, L. & Wernsdorfer, W. Molecular spintronics using single-molecule magnets. *Nature Mater.* **7**, 179–186 (2008).
17. Friedman, J. R., Sarachik, M. P., Tejada, J. & Ziolo, R. Macroscopic measurement of resonant magnetization tunnelling in high-spin molecules. *Phys. Rev. Lett.* **76**, 3830–3833 (1996).
18. Thomas, L. *et al.* Macroscopic quantum tunnelling of magnetization in a single crystal of nanomagnets. *Nature* **383**, 145–147 (1996).
19. Wernsdorfer, W. & Sessoli, R. Quantum phase interference and parity effects in magnetic molecular clusters. *Science* **284**, 133–135 (1999).
20. Ardavan, A. *et al.* Will spin-relaxation times in molecular magnets permit quantum information processing? *Phys. Rev. Lett.* **98**, 1–4 (2007).
21. Bertaina, S. *et al.* Quantum oscillations in a molecular magnet. *Nature* **453**, 203–206 (2008).
22. Komeda, T. *et al.* Observation and electric current control of a local spin in a single-molecule magnet. *Nature Commun.* **2**, 217 (2011).
23. Otte, A. F. *et al.* The role of magnetic anisotropy in the Kondo effect. *Nature Phys.* **4**, 847–850 (2008).
24. Heersche, H. B. *et al.* Electron transport through single Mn₁₂ molecular magnets. *Phys. Rev. Lett.* **96**, 206801 (2006).
25. Zyazin, A. S. *et al.* Electric field controlled magnetic anisotropy in a single molecule. *Nano Lett.* **10**, 3307–3311 (2010).
26. Urdampilleta, M., Cleuziou, J.-P., Klyatskaya, S., Ruben, M. & Wernsdorfer, W. Supramolecular spin valves. *Nature Mater.* **10**, 502–506 (2011).
27. Park, H., Lim, A. K. L., Alivisatos, A. P., Park, J. & McEuen, P. L. Fabrication of metallic electrodes with nanometer separation by electromigration. *Appl. Phys. Lett.* **75**, 301–303 (1999).
28. Stepanow, S. *et al.* Spin and orbital magnetic moment anisotropies of monodispersed bis(phthalocyaninato)terbium on a copper surface. *Supp. Inf. J. Am. Chem. Soc.* **132**, 11900–11901 (2010).
29. Ishikawa, N., Sugita, M. & Wernsdorfer, W. Quantum tunneling of magnetization in lanthanide single-molecule magnets: bis(phthalocyaninato)terbium and bis(phthalocyaninato)dysprosium anions. *Angew. Chem. Int. Ed.* **44**, 2931–2935 (2005).
30. Abragam, A. *The Principles of Nuclear Magnetism* (Oxford Univ. Press, 1994).
31. Leuenberger, M. N. & Loss, D. The Grover algorithm with large nuclear spins in semiconductors. *Phys. Rev. B* **68**, 165317 (2003).

Supplementary Information is linked to the online version of the paper at www.nature.com/nature.

Acknowledgements We thank E. Eyraud, D. Lepoittevin, L. Cagnon, R. Haettel, C. Hoarau, V. Reita and P. Rodière for technical contributions and discussions. We thank T. Fournier, T. Crozes, B. Fernandez, S. Dufresnes and G. Julie for lithography development; E. Bonet, C. Thirion and R. Piquere for help with software development and M. Urdampilleta, S. Thiele, N. Roch, A. Varlet and A. Ralko for discussions. Samples were fabricated in the Nanofab facility of the Néel Institute. This work is partially supported by the French National Research Agency National Programme in Nanosciences and Nanotechnologies (ANR-PNANO) project MolNanoSpin, number ANR-08-NANO-002; European Research Council Advanced Grant MolNanoSpin, number 226558; ICT-2007.8.0 Future Emerging Technologies Open, Quantum Information Processing Specific Targeted Research Project number 211284 MolSpinQIP; the German Research Foundation programme TRR 88 ‘3Met’; Cible 2009; and the Nanosciences Foundation of Grenoble.

Author Contributions R.V., W.W. and F.B. designed, conducted and analysed the experiments; S.K. and M.R. designed, synthesized and characterized the molecule; R.V., M.R., W.W., and F.B. co-wrote the paper.

Author Information Reprints and permissions information is available at www.nature.com/reprints. The authors declare no competing financial interests. Readers are welcome to comment on the online version of this article at www.nature.com/nature. Correspondence and requests for materials should be addressed to F.B. (franck.balestro@grenoble.cnrs.fr) or M.R. (mario.ruben@kit.edu).